Chemical Science

ROYAL SOCIETY OF CHEMISTRY

EDGE ARTICLE

View Article Online
View Journal | View Issue

Cite this: *Chem. Sci.*, 2026, **17**, 6467

All publication charges for this article have been paid for by the Royal Society of Chemistry

Received 29th October 2025
Accepted 27th January 2026

DOI: 10.1039/d5sc08373g

rsc.li/chemical-science

A mechanochemical route to triazatrinaphthylenes: building blocks for π-extended, nitrogen-enriched two-dimensional metal–organic frameworks

Rohan Mahapatra,[ab] Kalipada Koner,[ab] Ranajit Maity[ab] and Rahul Banerjee *[abc]

Nitrogen-containing polyaromatic heterocycles are the key molecular materials in semiconducting and optoelectronic devices, yet their synthesis typically depends on high-boiling, toxic organic solvents and multi-step catalytic processes. Herein, we report a metal-free solid-state synthetic strategy followed by thermal treatment for the efficient synthesis of the functionalized C_{3h}-symmetric triazatrinaphthylene (TNP) derivatives. Through rigorous optimisation of catalyst concentration, reaction stoichiometry, temperature, and time, this protocol delivers nearly quantitative yields (up to 95%) while eliminating hazardous solvents. The solid-state nature of the method also facilitated direct observation of the key reaction intermediates, such as mono- and tri-imine species, and partially cyclized products, providing mechanistic information for stepwise condensation and S_NAr-mediated aromatisation. Importantly, our synthetic approach allowed access to a hexa-hydroxy TNP ligand TNP(OH)$_6$, which was further employed to construct a two-dimensional Cu(II)-based metal–organic framework (Cu–TNP). The resulting MOF exhibits high crystallinity, efficient π–π stacking, and a BET surface area of 821 m^2 g^{-1}. This study showcases the utilisation of a solid-state synthetic route in accessing complex π-extended architectures and positions nitrogen-rich TNPs as versatile platforms for functional materials design.

Introduction

The polyaromatic heterocycles serve as a versatile class of π-conjugated molecular architectures that form central structural building blocks for organic electronics, optoelectronic materials, and porous structures.[1] They play a crucial role in the design of metal–organic frameworks, where their rigid π-conjugated backbones and heteroatom-rich coordination sites enable the construction of highly ordered and stable porous architectures. When incorporated as organic linkers, these units impart MOFs with tunable electronic structures, extended charge-delocalization pathways, and strong host–guest interactions, thereby expanding their utility beyond gas storage and separation to applications in electrocatalysis, photocatalysis, chemical sensing, and energy conversion.[2] Incorporation of heteroatoms, especially nitrogen, into such scaffolds can profoundly affect their electronic distribution, increase intermolecular interactions, and facilitate metal coordination, thus broadening their functionality in both molecular and material chemistry.[3] Within this family, C_3-symmetric nitrogen-heteroaromatic polyaromatics have garnered considerable interest.[4] Their planar, nitrogen-rich, disc-like topology enables efficient π–π stacking, facilitates crystalline ordering, and makes them ideal for integration into semiconducting platforms and building blocks for metal–organic frameworks (MOFs).[5] However, the synthesis of such polyaromatic heterocycles traditionally relies on stepwise Pd-catalysed cross-couplings or harsh solvothermal conditions employing high-boiling, toxic solvents, often with poor yields and limited substrate scope.[6] In this work, we have developed a solid-state synthetic strategy for triazatrinaphthylene (TNP) derivatives, a class of nitrogen-containing polyaromatic hydrocarbons, *via* mechanochemical grinding followed by thermal treatment. Mechanochemistry, by virtue of inducing chemical transformations through mechanical force, has recently emerged as a sustainable synthetic platform with minimal solvent consumption, high atom economy, and access to elusive reaction pathways (Table 6,SI).[7] While solvent-free synthetic methods have been widely used for materials assembly and coordination chemistry, their application in synthesising π-extended, multi-nitrogen organic frameworks remains scarce.[8] Through systematic optimisation of reactant stoichiometry, acid catalysts, and thermal post-treatment, we have increased the yield of TNP derivatives from 40–70% (solvothermal) to 80–95%, while simultaneously suppressing competitive β-keto enamine formation. In addition, the solid-state nature of the reaction offered an advantage to track the key intermediates (mono-imine, tri-imine, and cyclized species), which revealed

[a]*Department of Chemical Sciences, Indian Institute of Science Education and Research Kolkata, West Bengal-741246, India. E-mail: r.banerjee@iiserkol.ac.in*

[b]*Centre for Advanced Functional Materials, Indian Institute of Science Education and Research, Kolkata, Mohanpur 741246, India*

[c]*College of Science, Korea University, 145 Anam-ro, Seongbuk-gu, South Korea*

profound insights into the sequence of transformation, typically obscured in solution procedures. Leveraging the resulting $TNP(OH)_6$ derivative as a planar, C_{3h} symmetric ligand, we synthesised a highly crystalline two-dimensional Cu-based MOF exhibiting a BET surface area of 821 $m^2\ g^{-1}$. This work thus demonstrates the intersection of polyaromatic heterocycle design and mechanochemical synthesis to produce sustainable, structurally complex, and functionally rich materials.

Results and discussion

Aromatic nucleophilic substitution (S_NAr) reactions are widely employed as a versatile strategy for covalent coupling between electron-rich and deficient aromatic moieties *via* heteroatoms.[9] Conventionally, successful S_NAr transformations require the installation of strong electron-withdrawing groups in *ortho* and *para* positions relative to the leaving group, thereby rendering the aryl substrate sufficiently electrophilic.[10] Interestingly, our group recently demonstrated an unconventional S_NAr route between two electron-rich aromatic molecules,[6e] enabling the construction of polyaromatic heterocycles through *in situ* iminium intermediate formation. Specifically, despite the presence of three electron-donating methoxy substituents (+R effect), 2,4,6-trimethoxybenzene-1,3,5-tricarbaldehyde (Tp-OMe) (Fig. S1–S6) exhibits S_NAr reactivity upon formation of electrophilic iminium intermediates, which activate the adjacent methoxy-bearing carbon centers. Yet, in the traditional solution-phase reactions, this transformation is normally undermined by side reactions, especially the generation of undesired β-keto enamines and mono-TNP species, leading to reduced yields of the target polyaromatic products. To address these limitations, we developed a mechanochemical approach that significantly enhances the efficiency of the reaction. In this method, 0.1 mmol of Tp-OMe (25 mg) was ground with appropriate aniline derivatives in the presence of an acid catalyst for 25 minutes using a mortar and pestle. After grinding, the product was collected, and the ^{1}H NMR spectrum confirmed the formation of the tri-imine complex (Fig. S81 and S84). Under mechanochemical conditions, the reaction mixture consistently remains a dense, paste-like solid, even in the presence of liquid aniline substrates and acetic acid, due to rapid adsorption of the liquid components onto solid Tp-OMe. Such paste-like states are well documented in mechanochemistry and are effective in maintaining high local reactant concentrations and efficient mass transfer under solvent-minimal conditions (Fig. S13). The resulting mixture was then transferred to a glass vial and subjected to thermal treatment (90 °C) for 24 hours (Fig. 1a). Remarkably, this thermomechanical approach improved the yield from a previously reported 40–70% to 70–95%, depending on the substrate. For reaction optimisation, *p*-amylaniline was chosen as a model aniline derivative owing to the high solubility of the corresponding polyaromatic product, and yields were quantified using ^{1}H NMR with 1,3,5-trimethoxybenzene as an internal standard. We systematically optimized the reaction conditions by varying key parameters, including the equivalents of *p*-amylaniline, the acid catalyst and its concentration, catalyst amount, reaction temperature, and duration (Fig. 2). Reactions were conducted with varying equivalents of *p*-amylaniline in the presence of 500 μL of acetic acid (AcOH) at 120 °C for 24 hours, and the product yields were

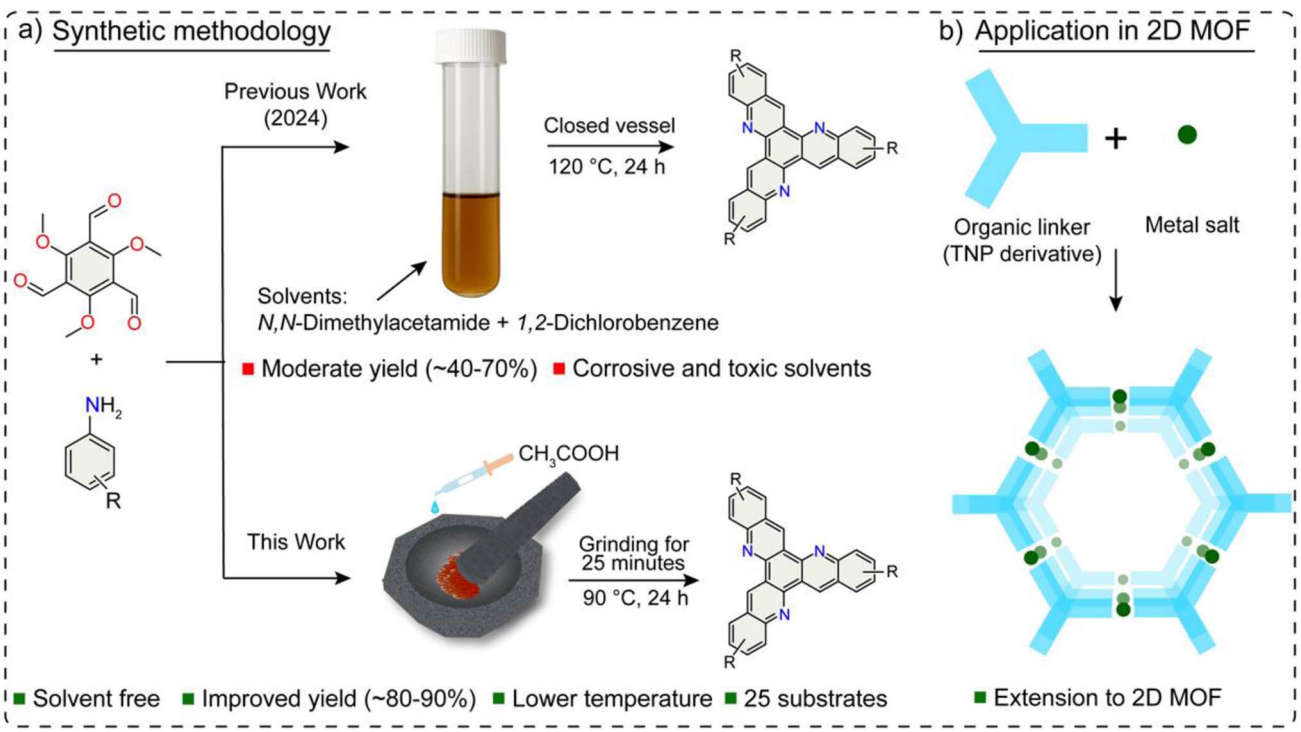

Fig. 1 (a) Synthetic methodology of triazatrinaphthylene derivatives; (b) synthesis of a Cu based metal organic framework from $TNP(OH)_6$.

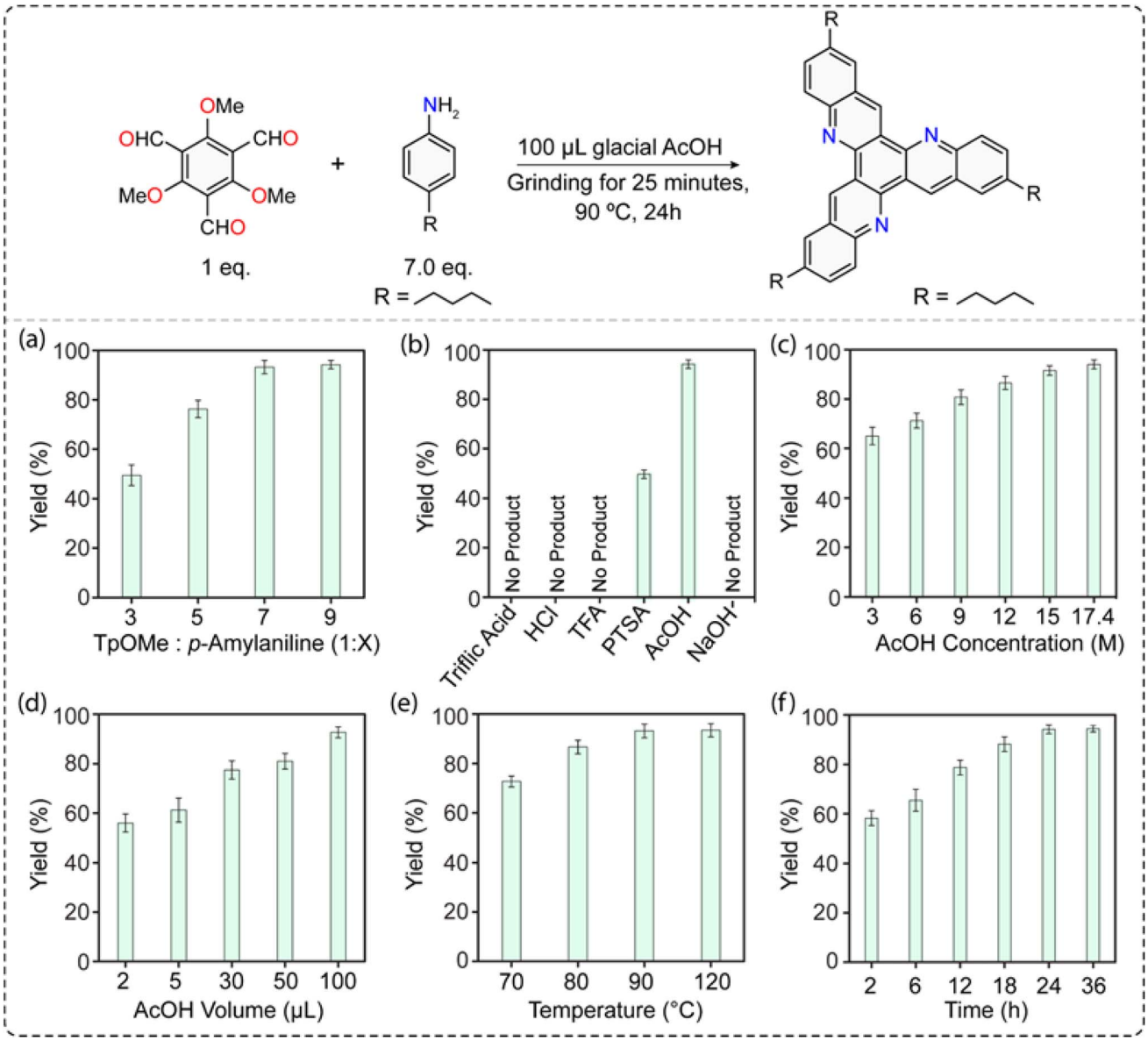

Fig. 2 Optimized yield was obtained by conducting the reaction between 2,4,6-trimethoxybenzene1,3,5-tricarbaldehyde, and *p*-amylaniline, (PAA), (a) % yield with different PAA equivalents, (b) % yield with different acids and bases, (c) % yield with acetic acid concentration, (d) % yield with acetic acid volume, (e) % yield at different temperatures, and (f) % yield at different times.

quantified *via* ^{1}H NMR spectroscopy. The crude ^{1}H NMR spectra revealed a characteristic singlet at δ 9.7 ppm, corresponding to the most deshielded aromatic C–H proton adjacent to the pyridinic nitrogen, alongside additional well-defined doublet–singlet–doublet patterns at δ 8.1, 7.8, and 7.6 ppm, respectively, consistent with the formation of the TNP–*p*-Amyl product (Fig. S22–S24). Beginning with 3 equivalents of *p*-amylaniline, we gradually increased the amount to 9 equivalents relative to the limiting aldehyde (Tp-OMe). The yield of the desired TNP–*p*-Amyl showed a clear dependence on amine stoichiometry, increasing from 49% at 3 equivalents to a maximum of 95% at 7 equivalents (Fig. 2a and S7). This trend can be accounted for by noting that three equivalents are required for Schiff base formation with the aldehyde groups, and the rest 3 eq. enables substitution of the methoxy groups through the S_NAr process. Although our initial hypothesis suggested that 6 equivalents of *p*-amylaniline would be necessary for complete cyclisation, given that each aromatic ring-forming event liberates three equivalents of aniline, the reaction still proceeded with moderate yield using only 3 equivalents, indicating a degree of equilibrium-driven tolerance (Fig. S14). To probe this behavior, Tp-OMe (0.40 mmol) was reacted with *p*-amylaniline (0.28 mmol) under the optimized conditions, after which unreacted *p*-amylaniline ($\approx$65 µL, 0.36 mmol) was recovered by chromatography and identified by ^{1}H NMR spectroscopy, supporting partial regeneration of the amine during the reaction (Fig. S19). Following stoichiometric optimisation, we screened a variety of Brønsted acids as catalysts. Among the acids tested, glacial

acetic acid consistently produced the highest yield (95%) of TNP–*p*-Amyl (Fig. S8). In contrast, *p*-toluenesulfonic acid afforded only a 52% yield, while stronger acids such as hydrochloric acid, triflic acid, and trifluoroacetic acid completely suppressed product formation by promoting rapid *in situ* demethylation of the transient tri-imine intermediate, followed by tautomerization to a thermodynamically stable β-keto enamine, thereby diverting the reaction from the productive cyclization pathway. In contrast, acetic acid provides a sufficiently mild acidic environment to enable efficient imine formation while avoiding premature demethylation (Fig. S15–S17). Notably, no product was observed under basic conditions using NaOH. Such Brønsted acid-dependent reactivity suggests involvement of a proton in the reaction pathway (Fig. 2b and S8). To further probe the influence of acid concentration, we investigated a series of acetic acid solutions ranging from 3 M to 17.4 M (glacial AcOH). The acid concentration was clearly correlated with product yield, highlighting the significance of proton activity that expedites the reaction sequence. The yield of the desired TNP derivative exhibited a dependence on acid concentration, increasing from 65% to 95% as the concentration of acetic acid was increased from 3 M to 17.4 M (glacial acetic acid) (Fig. 2c and S9). This trend reflects the effect of acid dilution: dilution of acetic acid significantly influences the reaction outcome by increasing water activity in the medium. While glacial acetic acid provides near-anhydrous conditions that strongly favor imine condensation, diluted acetic acid partially shifts the equilibrium toward imine hydrolysis, leading to reduced but still appreciable yields. Thus, the superior performance of glacial acetic acid arises from its low water content, which suppresses hydrolytic back-reactions and stabilizes the reactive imine intermediates (Fig. S18). In addition to acid concentration, acid stoichiometry also played a crucial role in dictating reaction efficiency. We observed a progressive increase in the yield when the volume of glacial acetic acid was adjusted between 2 μL and 100 μL, reaching a maximum yield of 95% (Fig. 2d and S10). With the catalytic conditions already optimised, we then explored the role of temperature and reaction time in the formation of products. Temperature had a relatively weaker impact on the polyaromatization outcome. Increasing the reaction temperature from 70 °C to 120 °C improved the yield from 80% to 95% (Fig. 2e and S11), which suggests that key intermediates may already form during the initial mechanochemical grinding, requiring only mild thermal energy to complete cyclisation. This hypothesis was further supported by time-dependent experiments. The TNP product was isolable in 60% yield after just 2 hours of heating, and the yield gradually increased to 95% upon extending the reaction time to 24 hours (Fig. 2f and S12). With a robust and high-yielding solid-state protocol in place, we turned our attention to substrate scope. We introduced a series of aniline derivatives bearing diverse substituents to gain deeper insight into the electronic and steric influences on the reaction pathway. Electron-donating substituents positioned *ortho*, *meta*, and *para* to the amine functionality consistently afforded high yields (78–95%), while unsubstituted aniline furnished the corresponding TNP in 70% yield; alkyl-substituted anilines such as methyl (80%), propyl (93%), butyl (82%), isopropyl (94%), Amyl, and *tert*-butyl demonstrated a consistent trend of increasing yields, reaching up to 95% (Fig. S72–S79). This enhancement is attributed to their positive inductive effects (+I), which likely enhance the nucleophilicity of amines and facilitate nucleophilic aromatic substitution. Encouraged by these results, we explored substituents with distinctive electronic characteristics, including *para*-methoxy, phenoxy, and trifluoromethoxy groups, which combine the negative inductive effect (−I) with the positive mesomeric effect (+M). Introduction of a strongly electron-withdrawing group resulted in a noticeable decrease in yield to 80%, underscoring the reaction's sensitivity to electronic effects on the nucleophilic aniline partner. We further expanded the substrate scope by synthesising TNP derivatives bearing heteroatom-rich functionalities, such as *N*,*N*-dimethylamine (–NMe_2) and morpholine. The morpholine-substituted TNP was obtained in higher yield (88%) compared to its NMe_2 analogue (80%). In this S_NAr-based cyclization, the nucleophilicity of the aniline plays a central role. Anilines bearing electron-donating groups (+M/+I effect) possess higher electron density on the amino nitrogen, which promotes nucleophilic attack and thus facilitates the overall transformation. In contrast, anilines substituted with electron-withdrawing groups (−M/−I effects) show reduced electron density on the nitrogen, resulting in slower cyclization compared with their electron-rich counterparts. To investigate steric effects, we examined *meta*- and *ortho*-substituted anilines. Both *meta*-isopropyl and *tert*-butyl anilines gave products in 95% (NMR yield). In contrast, *ortho*-methyl substitution led to yields similar to those of *para*-substituted analogues, while the yield using *ortho*-ethyl aniline declined considerably. This drop is presumably because steric overcrowding about the iminium cation centre hinders efficient cyclisation. To demonstrate the synthetic breadth of this methodology, we also synthesised disubstituted TNP derivatives, including $TNP(Me)_6$ and $TNP(OMe)_6$, which were obtained in slightly reduced yields of 73% and 70%, respectively. Finally, we have further extended the π annulation by incorporating a naphthalene core, which enhances both π-conjugation and molecular complexity (Fig. 3 and S20–S71).

Mechanistic investigation

In pursuit of more profound insight into the mechanism, we selected *p*-butylaniline as the benchmark substrate and analysed the intermediates using high-resolution mass spectrometry (HRMS). To monitor the reaction under mechanochemical grinding, Tp-OMe and *p*-butylaniline were first ground together, and the resulting solid mixture was subjected to HRMS analysis. A prominent molecular ion peak at *m*/*z* 384.1865 $[M + H]^+$ (Fig. 4a and S83) was observed, consistent with the formation of a mono-imine intermediate (I), a product of the initial condensation between the aldehyde and amine groups. Further grinding of the mixture led to the appearance of a new peak at *m*/*z* 646.4009 $[M + H]^+$ (Fig. 4b and S84), corresponding to the tri-imine intermediate (Fig. S81), indicating the progression of the reaction under purely mechanochemical grinding. These

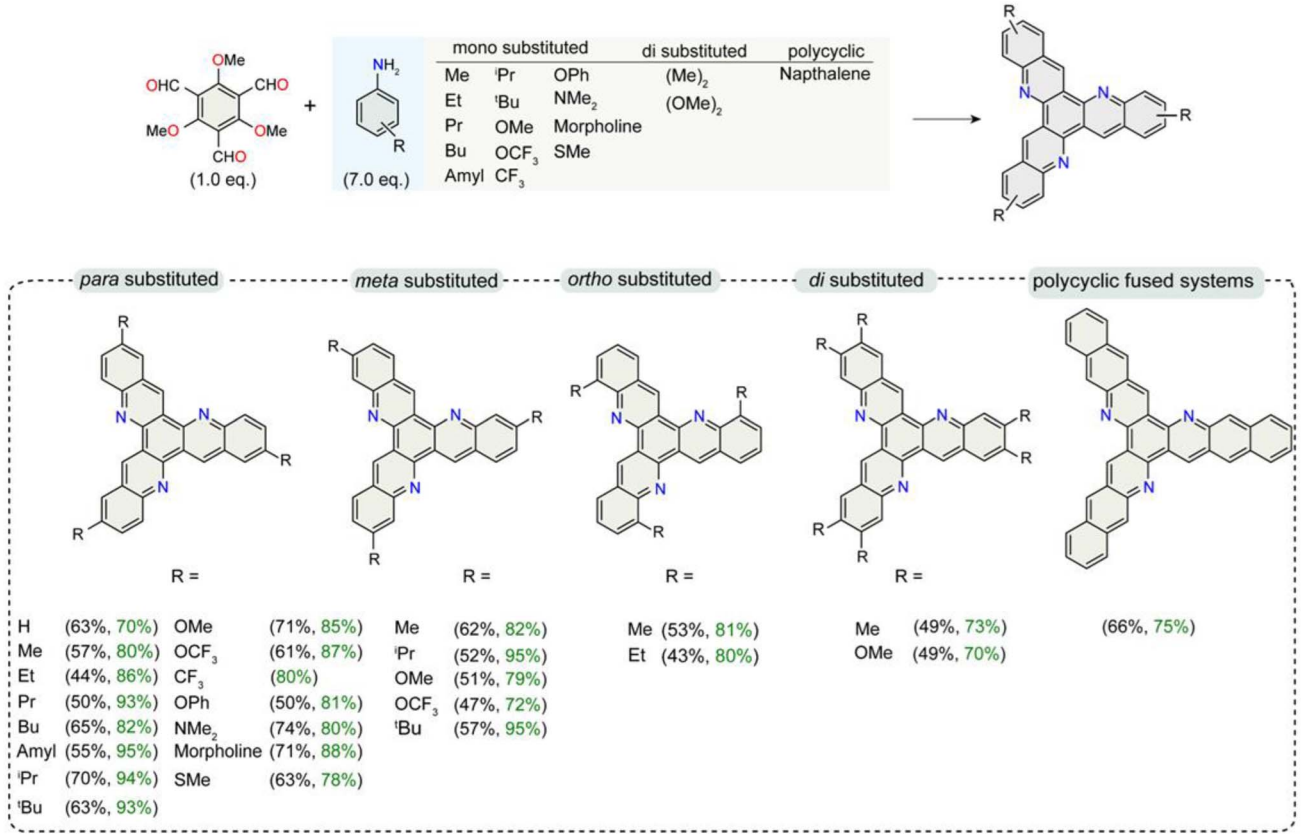

Fig. 3 Substrate scope; all the reactions were performed with 0.1 mmol of 2,4,6-trimethoxybenzene-1,3,5-tricarbaldehyde and 0.7 mmol of different aniline derivatives. Black colour % yield denotes the yield from solvothermal synthesis, and green colour % yield denotes the yield from mechanochemical synthesis. For R = H, Me, OMe, OCF_3, CF_3, OPh, NMe_2, Morpholine, SMe, $(Me)_2$, $(OMe)_2$, naphthyl, as the corresponding TNP compounds are partially soluble in any deuterated solvent, the isolated yield was considered. The NMR yields for R = Et, pr, Bu, Amyl, ^{i}Pr, ^{t}Bu are provided in the SI (Fig. S72–S79).

tri-imine species serve as key precursors in the ring-closing cyclisation steps, which are facilitated in the presence of Brønsted acid catalysts that promote iminium intermediate formation. However, the formation of the fully fused aromatic TNP core requires additional energy input to enable aromatic nucleophilic substitution and intramolecular Friedel–Crafts-type cyclisation. To drive these transformations, we thermally treated the ground mixture at 90 °C for 10 minutes. Post-heating HRMS revealed a distinct new intermediate and assessed the peak at m/z 848.5656 $[M + H]^+$ (Fig. 4c and S85), attributed to a mono-cyclized di-imine intermediate (III), confirming partial ring fusion. To further validate the role of imine steric influences in cyclisation, we examined reactions with sterically hindered aniline derivatives, specifically 2,6-dimethyl aniline. The ^{1}H NMR spectra displayed a singlet at δ 8.5 ppm, indicative of exclusive tri-imine formation without subsequent cyclisation, underscoring the importance of steric accessibility around the reactive centres (Fig. S80). Additionally, the appearance of the m/z 848.5656 peak in HRMS supports the hypothesis that S_NAr substitution occurs only after iminium formation. To prove our hypothesis, we performed additional control experiments to better understand the sequence of events. First, we synthesized the tri-imine intermediate by reacting 1 equivalent of Tp-OMe aldehyde with 3 equivalents of *p*-butyl aniline. In the crude NMR spectrum, the characteristic imine signal appears at approximately δ 8.8 ppm, confirming the successful formation of the tri-imine species. Next, we introduced an additional 3 equivalents of *p*-Amyl aniline to this crude imine mixture. Under these conditions, we obtained the corresponding TNP product (Fig. S81 and S82). Since the methoxy groups on Tp-OMe are strongly electron-donating, S_NAr is unlikely to proceed in their presence due to insufficient stabilization of the Meisenheimer complex. However, once the electron-withdrawing iminium functionality is introduced, the aromatic ring becomes sufficiently electrophilic to permit efficient nucleophilic substitution by aniline derivatives.[11] Thus the TNP derivatives with electron-donating groups such as hydroxyl offer significant advantages in coordination-driven assembly: they enhance ligand binding to metal nodes, promote the formation of robust metal–ligand coordination bonds, and facilitate the construction of highly connected frameworks.

Two-dimensional metal organic frameworks

To illustrate the general applicability of this solid-state procedure, we prepared $TNP(OH)_6$, a C_{3h}-symmetric ligand intended for use in the assembly of two-dimensional (2D) metal–organic

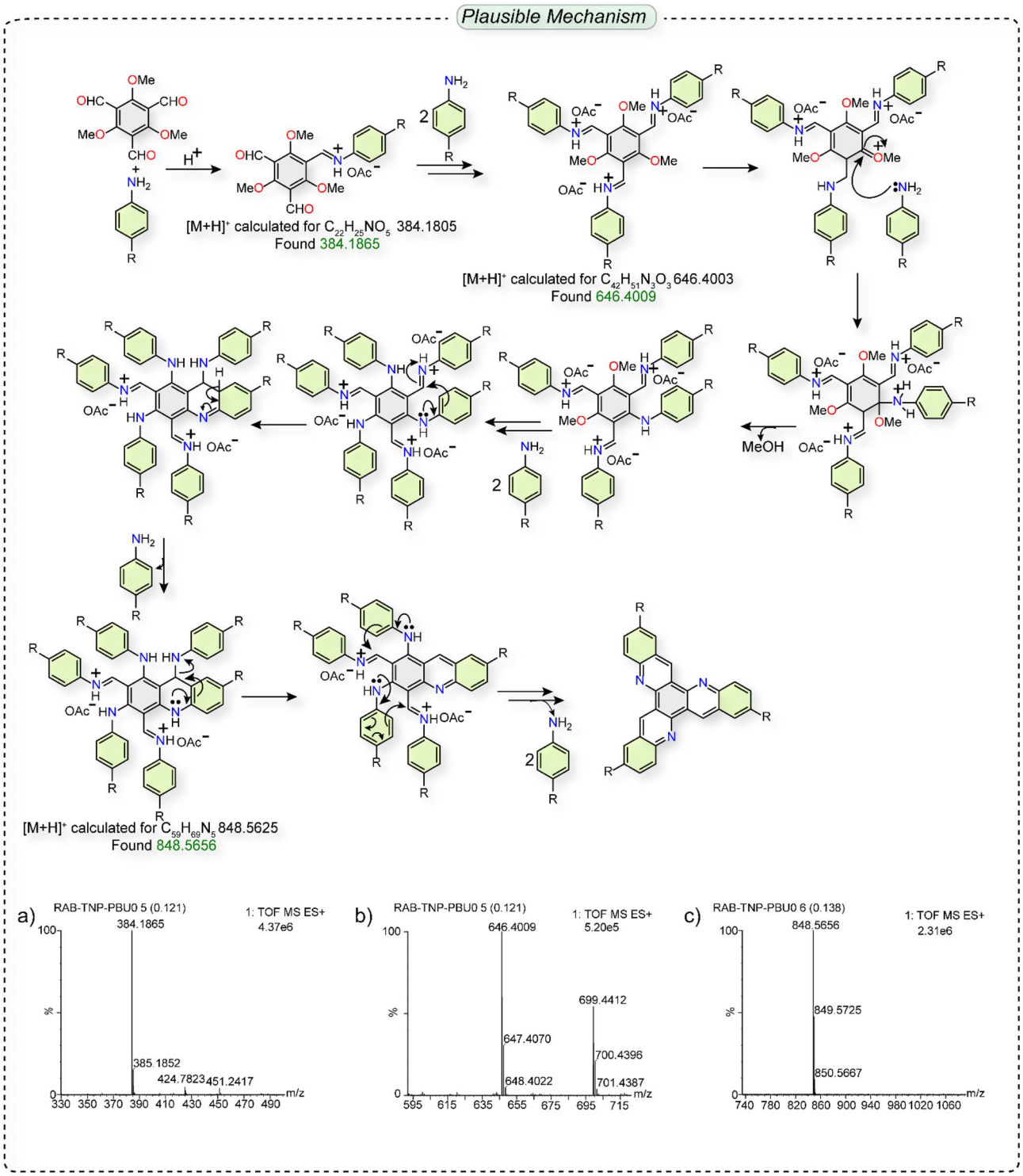

Fig. 4 Mechanistic investigation HRMS of the (a) monoimine intermediate, (b) tri-imine intermediate, and (c) intermediate (III) after one side ring formation. Here intermediate studies have been performed with R = *p*-butyl aniline.

frameworks (MOFs). The planarity and extended π-conjugation of the TNP core were anticipated to promote strong π–π stacking interactions, an important consideration in the assembly of layered 2D structures. Nonetheless, the symmetric positioning of coordinating groups like hydroxyl (–OH), amine (–NH_2), and thiol (–SH) directly onto the TNP framework poses synthetic difficulties since such nucleophilic functionalities can either interfere with the S_NAr reaction pathway or render the polyaromatization inefficient. To circumvent this problem, we strategically introduced six methoxy (–OMe) groups at the

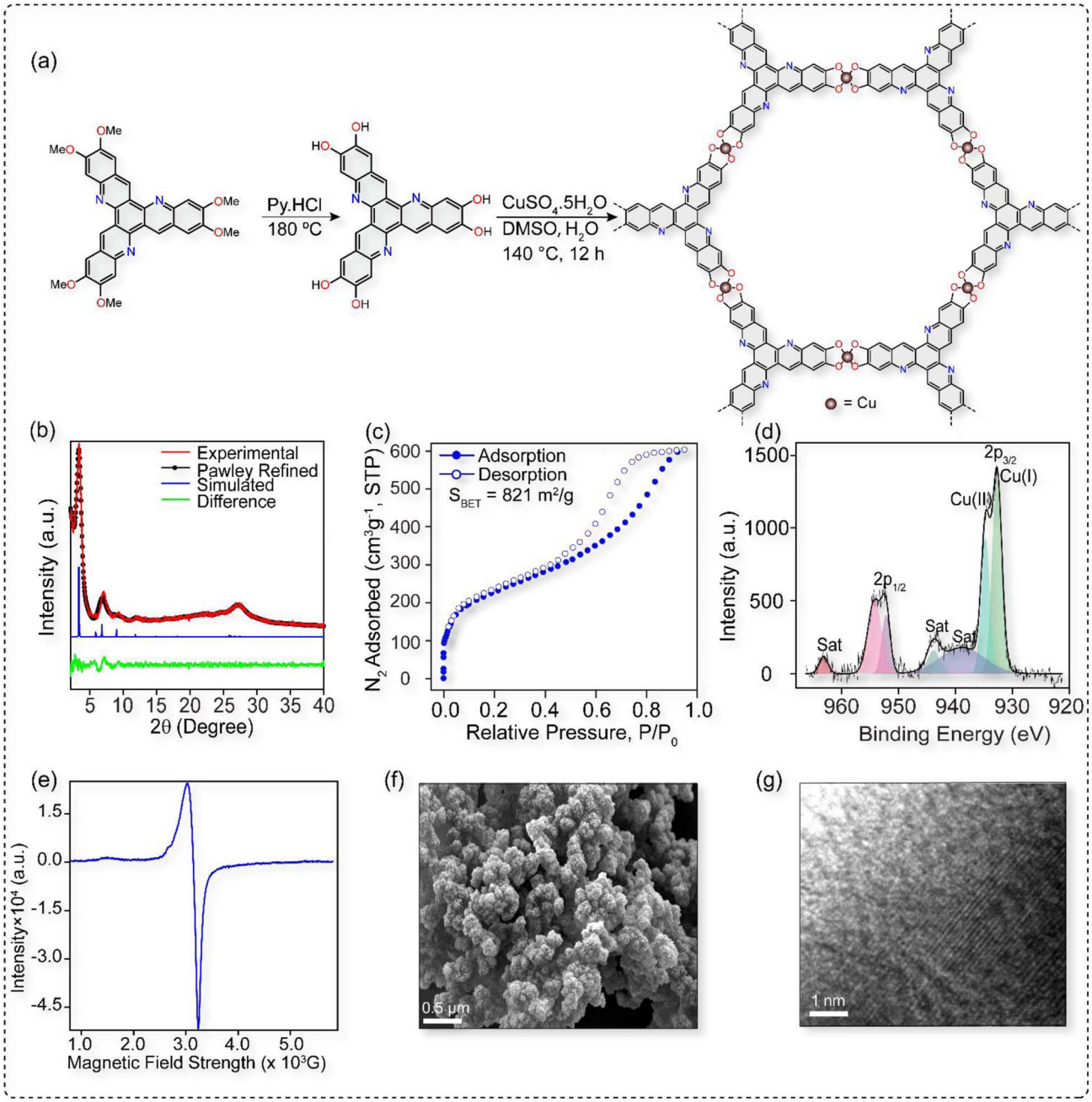

Fig. 5 (a) Synthetic scheme of the $TNP(OH)_6$ ligand and metal organic framework, (b) powder X-ray diffraction pattern, (c) N_2 adsorption isotherm, (d) XPS spectra, (e) electron paramagnetic resonance spectrum, (f) SEM image, and (g) HRTEM image of Cu–TNP MOF.

periphery of the molecule. This not only masked the nucleophilicity of the oxygen atoms but also enhanced the overall yield of $TNP(OMe)_6$ *via* the +M effect. The resulting compound was then subjected to demethylation using pyridine hydrochloride[12] at 180 °C, affording the hexahydroxy analogue $TNP(OH)_6$,[13] having a distinctive peak at δ 10.42 and 10.05 in ^{1}H NMR spectroscopy, attributed to two types of hydroxy groups (Fig. S87). There is a characteristic peak at 3344 cm^{-1} attributed to the OH functionality (Fig. S90). We selected Cu(II) as the coordinating metal, inspired by its successful use in 2D MOFs featuring hexahydroxytriphenylene (HHTP)[1] hexaaminotetraazatetranaphthotetraphene (HITT),[14] and their hydroxy analogues (HHTT).[15] In our synthetic protocol, $TNP(OH)_6$ was reacted with $CuSO_4 \cdot 5H_2O$ to yield the desired MOF (Fig. 5a). Powder X-ray powder diffraction (PXRD) and Pawley refinement confirmed that Cu–TNP crystallizes in the hexagonal space group $P6_3/m$, with unit cell parameters: a = 29.8 Å, b = 29.8 Å, and c = 6.9 Å, and $\alpha = \beta = 90°$, and $\gamma = 120°$. A distinct diffraction peak at 2θ = 3.39°, indexed to the (100) plane, reflects long-range in-plane order, consistent with the formation of stacked 2D architecture (Fig. 5b, S91 and S92). In the structure, the Cu^{2+} sites are bound by four oxygen atoms of

the catecholate fragments with a square planar geometry. This coordination mode not only facilitates the development of 2D layers but also fosters π–π stacking interactions among neighbouring sheets and thus increases crystallinity and structural durability. Nitrogen adsorption isotherms at 77 K revealed a Brunauer–Emmett–Teller (BET) surface area of 821 $m^2\ g^{-1}$ (Fig. 5c, S93 and S94).[16] Furthermore, quenched solid density functional theory (QSDFT) analysis of the adsorption data showed a narrow pore size distribution centred at ∼21 Å, consistent with the designed framework topology (Fig. S95). To probe the electronic environment of the metal centres, electron paramagnetic resonance (EPR) spectroscopy was performed. The spectrum displayed characteristic g-values ($g_x = g_y = 2.1$; $g_z = 2.3$; $g_{avg} = 2.17$), indicative of Cu(II) species in a square planar environment (Fig. 5e). EPR detects only paramagnetic Cu(II) species since Cu(I) is diamagnetic and EPR silent. X-ray photoelectron spectroscopy (XPS) further ascertained the elemental composition, revealing signals corresponding to C, N, O, and Cu. Notably, the high-resolution Cu 2p spectra indicated the presence of mixed-valent Cu^{2+} (934.71 eV) and Cu^{+} (932.78 eV) species.[17] Deconvolution of the N 1s spectrum revealed a predominant peak for C=N bonds, consistent with the triazatrinaphthylene core (Fig. 5d, S97 and S98). The optical band gap of the Cu–TNP MOF was determined using UV-vis spectroscopy combined with Kubelka–Munk analysis. The material shows strong visible-light absorption with a broad band spanning ∼450–800 nm and an absorption maximum at ∼570 nm, corresponding to an optical transition energy of ∼2.17 eV. Consistently, linear extrapolation of the $(F(R)h\nu)^2$ *versus* $h\nu$ plot gives a band gap of 2.14 eV, confirming the semiconducting nature of the Cu–TNP MOF (Fig. S99). SEM images reveal a well-defined, flower-like aggregated morphology (Fig. 5f and S100). The HRTEM image shows distinct lattice fringes extending over a few nanometers, confirming the presence of locally ordered crystalline domains embedded within a less ordered matrix (Fig. S5g). These results establish Cu–TNP MOF as a π-conjugated, nitrogen-rich 2D material with high crystallinity, porosity, and mixed-valence character.

Conclusions

In summary, we have developed a green and metal-free solid state thermomechanical synthesis of C_{3h} symmetric triazatrinaphthylene (TNP) building blocks with a wide substrate scope and excellent functional group tolerance. This solvent-free methodology provides significantly higher yields (∼95%) than conventional solvothermal methods, along with deeper mechanistic understanding. Through extensive ^{1}H NMR and HRMS studies, we identified a few key intermediates, pointing out that the reaction moves forward *via* sequential imine bond formation, followed by S_NAr and ring cyclization. Trapping the key intermediates allows understanding the stepwise formation of the π-conjugated system. We further extended this synthetic platform to construct a two-dimensional copper-based metal–organic framework, thereby demonstrating the downstream relevance and practical utility of the hexa-hydroxy TNP ligand. The successful integration of this ligand into a 2D Cu-based framework highlights its effectiveness as a versatile building block for MOF construction, while the primary emphasis of this work remains on the development of the synthetic strategy and molecular design. This material exhibits high crystallinity, a large surface area (821 $m^2\ g^{-1}$), and a mixed-valence Cu^{2+}/Cu^{+} coordination environment. The synergy between extended π-conjugation, open metal sites, and high porosity makes Cu–TNP a promising candidate for electrocatalysis, charge transport, and sensing applications. Overall, this study provides a sustainable route to synthesize complex π-systems under ambient conditions and introduces a versatile building block for constructing functional porous frameworks, demonstrating the powerful intersection of organic synthesis, mechanochemistry, and reticular chemistry. However, the key transformation proceeds through an S_NAr pathway that requires an electron-rich amine nucleophile. Anilines bearing strong electron-withdrawing substituents, such as nitro or carboxylic acid groups, significantly reduce the nucleophilicity of the amine, thereby suppressing the S_NAr reactivity. As a result, the substrate scope of TNP derivatives for MOF synthesis is inherently constrained by the electronic nature of the substituents.

Author contributions

R. B. and R. M. conceived the idea of the project. R. M. synthesised and characterised the TNP derivatives and metal–organic framework. R. M. and R. J. M. have performed the data analysis. The manuscript was written with contributions from R. M., K. P. K. and R. B. All authors have given approval to the final version of the manuscript.

Conflicts of interest

There are no conflicts to declare.

Data availability

All data supporting the findings of this study are included in the main manuscript and the supporting information (SI). Additional experimental details and raw data files are available from the corresponding author upon reasonable request.

Supplementary information is available. See DOI: https://doi.org/10.1039/d5sc08373g.

Acknowledgements

RM acknowledges CSIR [File No.: 09/092 1(17568)/2024-EMR-I] for a Research Fellowship. RJM acknowledges UGC for a Research Fellowship. RM acknowledges R. B. for the funding from the DST Project; DST/C3E/MI2.0/CCUS/2K23/CALL/2023/153, submitted against FOA R&D in the area of CCUS with Mission Innovation.

Notes and references

1 (*a*) A. Pareek, M. Y. Mehboob, M. Cieplak, M. Majdecki, H. Szabat, K. Noworyta, P. Połczyński, M. Morawiak,

P. S. Sharma and C. Foroutan-Nejad, *J. Am. Chem. Soc.*, 2025, **147**, 5996–6005; (*b*) J. E. Anthony, *Chem. Rev.*, 2006, **106**, 5028–5048; (*c*) J. E. Anthony, *Angew. Chem., Int. Ed.*, 2008, **47**, 452–483; (*d*) K. Tuong Ly, R.-W. Chen-Cheng, H.-W. Lin, Y.-J. Shiau, S.-H. Liu, P.-T. Chou, C.-S. Tsao, Y.-C. Huang and Y. Chi, *Nat. Photonics*, 2017, **11**, 63–68; (*e*) X.-C. Li, H. Sirringhaus, F. Garnier, A. B. Holmes, S. C. Moratti, N. Feeder, W. Clegg, S. J. Teat and R. H. Friend, *J. Am. Chem. Soc.*, 1998, **120**, 2206–2207; (*f*) Y. Hu, G. M. Paternò, X.-Y. Wang, X.-C. Wang, M. Guizzardi, Q. Chen, D. Schollmeyer, X.-Y. Cao, G. Cerullo and F. Scotognella, *J. Am. Chem. Soc.*, 2019, **141**, 12797–12803; (*g*) Y. Yu, J. Wang, Y. Cui, Z. Chen, T. Zhang, Y. Xiao, W. Wang, J. Wang, X.-T. Hao and J. Hou, *J. Am. Chem. Soc.*, 2024, **146**, 8697–8705; (*h*) W. Zhao, S. Li, H. Yao, S. Zhang, Y. Zhang, B. Yang and J. Hou, *J. Am. Chem. Soc.*, 2017, **139**, 7148–7151; (*i*) M. Stepien, E. Gonka, M. Żyła and N. Sprutta, *Chem. Rev.*, 2017, **117**, 3479–3716.

2 (*a*) L. Yang, S. Kinoshita, T. Yamada, S. Kanda, H. Kitagawa, M. Tokunaga, T. Ishimoto, T. Ogura, R. Nagumo, A. Miyamoto and M. Koyama, *Angew. Chem., Int. Ed.*, 2010, **49**, 5348–5351; (*b*) M. Zhou, Y. Zhang, H. Li, Z. Li, S. Wang, X. Lu and S. Yang, *Angew. Chem., Int. Ed.*, 2025, **64**, e202414392; (*c*) H. Guo, D. Si, H. Zhu, Z. Chen, R. Cao and Y. Huang, *Angew. Chem., Int. Ed.*, 2024, **136**, e202319472; (*d*) K. Saravanan, M. Nagarathinam, P. Balaya and J. J. Vittal, *J. Mater. Chem.*, 2010, **20**, 8329; (*e*) Z. Chang, H. Yang, X. Zhu, P. He and H. Zhou, *Nat. Commun.*, 2022, **13**, 1510; (*f*) S. Navalón, A. Dhakshinamoorthy, M. Álvaro, B. Ferrer and H. García, *Chem. Rev.*, 2023, **123**, 445–490; (*g*) X. Peng, X. Wu, M. Zhang and H. Yuan, *ACS Sens.*, 2023, **8**, 2471–2492.

3 (*a*) X.-Y. Wang, X. Yao, A. Narita and K. Müllen, *Acc. Chem. Res.*, 2019, **52**, 2491–2505; (*b*) B. Li, Y. Qu, J. Lou, L. Liu, Y. Huang, H. Zhang, B. Z. Tang and Z. Wang, *Angew. Chem., Int. Ed.*, 2025, e202506504.

4 (*a*) R. Chowdhury, M. D. Preuss, H.-H. Cho, J. J. Thompson, S. Sen, T. K. Baikie, P. Ghosh, Y. Boeije, X. W. Chua and K.-W. Chang, *Science*, 2025, **387**, 1175–1181; (*b*) Y. J. Cho, K. S. Yook and J. Y. Lee, *Adv. Mater.*, 2014, **26**, 4050–4055.

5 (*a*) C. Lu, J. Y. Choi, B. Check, X. Fang, S. Spotts, D. Nunez and J. Park, *J. Am. Chem. Soc.*, 2024, **146**, 26313–26319; (*b*) H. T. Pham, J. Y. Choi, S. Huang, X. Wang, A. Claman, M. Stodolka, S. Yazdi, S. Sharma, W. Zhang and J. Park, *J. Am. Chem. Soc.*, 2022, **144**, 10615–10621; (*c*) G. Lee, G. Park and S. S. Park, *J. Am. Chem. Soc.*, 2024, **146**, 29767–29772; (*d*) T. Chen, H. Li, X. Shi, J. Imbrogno and D. Zhao, *J. Am. Chem. Soc.*, 2024, **146**, 14433–14438; (*e*) B. Song, Y. Liang, Y. Zhou, L. Zhang, H. Li, N.-X. Zhu, B. Z. Tang, D. Zhao and B. Liu, *J. Am. Chem. Soc.*, 2024, **146**, 14835–14843; (*f*) Z. Yan, Y. Bai, S. Zhang, L. Kong, Y. Wang, H. Sun, Y. Li, L. Qiu, R. Zhang, P. Jiang, D. Zhao, Z. Chen, Y. Li, H. Pang and J. Wang, *Nat. Commun.*, 2025, **16**, 2290; (*g*) Z. Yang, H. Lu, Q. Li, X. Guo, Q. Li, H. Zhou, B. Wang, Y. Qi, H. Chen, M. Yang, T. Tian, H. Yang, J. Ding and H. Pang, *Adv. Mater.*, 2025, e12289; (*h*) L. Su, H. Wu, S. Zhou, R. Qian, C. Cui, S. Zhang, L. Wu, W. Li and H. Pang, *Adv. Sci.*, 2025, e13616; (*i*) Z. Liu, W. Feng, H. Xu, Z. Yang, W. Li, M. Shakouri, H. Chen, F. Zhang and H. Pang, *Adv. Sci.*, 2025, e15034.

6 (*a*) R. C. Larock, M. J. Doty, Q. Tian and J. M. Zenner, *J. Org. Chem.*, 1997, **62**, 7536–7537; (*b*) Q. Li, C. Moussallem, F. Castet, L. Muccioli, M.-A. Dourges, T. Toupance and Y. Nicolas, *Org. Lett.*, 2021, **24**, 344–348; (*c*) H. Bertrand, A. Granzhan, D. Monchaud, N. Saettel, R. Guillot, S. Clifford, A. Guédin, J. L. Mergny and M. P. Teulade-Fichou, *Chem.–Eur. J.*, 2011, **17**, 4529–4539; (*d*) H. Bertrand, R. Guillot, M. P. Teulade-Fichou and D. Fichou, *Chem.–Eur. J.*, 2013, **19**, 14654–14664; (*e*) N. Saettel, N. Katsonis, A. Marchenko, M.-P. Teulade-Fichou and D. Fichou, *J. Mater. Chem.*, 2005, **15**, 3175–3180; (*f*) Q. Feng, Z. Fan, T. Ruizhi, F. Yubin, W. Xinyang, H. Sheng, Z. Xiaodong and F. Xinliang, *Org. Lett.*, 2016, **18**, 1398–1401; (*g*) X. Tian, K. Shoyama and F. Würthner, *Chem. Sci.*, 2023, **14**, 284–290; (*h*) K. Koner and R. Banerjee, *Nat. Synth.*, 2024, **3**, 1266–1274.

7 (*a*) S. L. James, C. J. Adams, C. Bolm, D. Braga, P. Collier, T. Friščić, F. Grepioni, K. D. Harris, G. Hyett and W. Jones, *Chem. Soc. Rev.*, 2012, **41**, 413–447; (*b*) T. Seo, K. Kubota and H. Ito, *J. Am. Chem. Soc.*, 2023, **145**, 6823–6837; (*c*) Y. Lin, T. B. Kouznetsova, A. G. Foret and S. L. Craig, *J. Am. Chem. Soc.*, 2024, **146**, 3920–3925.

8 (*a*) J.-L. Do and T. Friščić, *ACS Cent. Sci.*, 2017, **3**, 13–19; (*b*) P. J. Beldon, L. Fábián, R. S. Stein, A. Thirumurugan, A. K. Cheetham and T. Friščić, *Angew. Chem., Int. Ed.*, 2010, **49**, 9640–9643.

9 S. Rohrbach, A. J. Smith, J. H. Pang, D. L. Poole, T. Tuttle, S. Chiba and J. A. Murphy, *Angew. Chem., Int. Ed.*, 2019, **58**, 16368–16388.

10 M. Shigeno, K. Hayashi, O. Sasamoto, R. Hirasawa, T. Korenaga, S. Ishida, K. Nozawa-Kumada and Y. Kondo, *J. Am. Chem. Soc.*, 2024, **146**, 32452–32462.

11 J. W. Greenwood, M. A. Larsen, S. A. Burgess, J. A. Newman, Y. Jiang and A. C. Sather, *Nat. Synth.*, 2023, **2**, 1059–1067.

12 P. P. Kulkarni, A. J. Kadam, R. B. Mane, U. V. Desai and P. P. Wadgaonkar, *J. Chem. Res., Synop.*, 1999, 394–395.

13 (*a*) A. M. Eagleton, M. Ko, R. M. Stolz, N. Vereshchuk, Z. Meng, L. Mendecki, A. M. Levenson, C. Huang, K. C. MacVeagh and A. Mahdavi-Shakib, *J. Am. Chem. Soc.*, 2022, **144**, 23297–23312; (*b*) Y.-M. Jo, K. Lim, J. W. Yoon, Y. K. Jo, Y. K. Moon, H. W. Jang and J.-H. Lee, *ACS Cent. Sci.*, 2021, **7**, 1176–1182; (*c*) K. M. Snook, L. B. Zasada, D. Chehada and D. J. Xiao, *Chem. Sci.*, 2022, **13**, 10472–10478; (*d*) R. W. Day, D. K. Bediako, M. Rezaee, L. R. Parent, G. Skorupskii, M. Q. Arguilla, C. H. Hendon, I. Stassen, N. C. Gianneschi and P. Kim, *ACS Cent. Sci.*, 2019, **5**, 1959–1964.

14 J. Wang, T. Chen, M. Jeon, J. J. Oppenheim, B. Tan, J. Kim and M. Dinca, *J. Am. Chem. Soc.*, 2024, **146**, 20500–20507.

15 J.-H. Dou, M. Q. Arguilla, Y. Luo, J. Li, W. Zhang, L. Sun, J. L. Mancuso, L. Yang, T. Chen, L. R. Parent, G. Skorupskii, N. J. Libretto, C. Sun, M. C. Yang, P. V. Dip, E. J. Brignole, J. T. Miller, J. Kong, C. H. Hendon, J. Sun and M. Dincă, *Nat. Mater.*, 2021, **20**, 222–228.

16 J. W. M. Osterrieth, J. Rampersad, D. Madden, N. Rampal, L. Skoric, B. Connolly, M. D. Allendorf, V. Stavila, J. L. Snider, R. Ameloot, J. Marreiros, C. Ania, D. Azevedo, E. Vilarrasa-Garcia, B. F. Santos, X. Bu, Z. Chang, H. Bunzen, N. R. Champness, S. L. Griffin, B. Chen, R. Lin, B. Coasne, S. Cohen, J. C. Moreton, Y. J. Colón, L. Chen, R. Clowes, F. Coudert, Y. Cui, B. Hou, D. M. D'Alessandro, P. W. Doheny, M. Dincă, C. Sun, C. Doonan, M. T. Huxley, J. D. Evans, P. Falcaro, R. Ricco, O. Farha, K. B. Idrees, T. Islamoglu, P. Feng, H. Yang, R. S. Forgan, D. Bara, S. Furukawa, E. Sanchez, J. Gascon, S. Telalović, S. K. Ghosh, S. Mukherjee, M. R. Hill, M. M. Sadiq, P. Horcajada, P. Salcedo-Abraira, K. Kaneko, R. Kukobat, J. Kenvin, S. Keskin, S. Kitagawa, K. Otake, R. P. Lively, S. J. A. DeWitt, P. Llewellyn, B. V. Lotsch, S. T. Emmerling, A. M. Pütz, C. Martí-Gastaldo, N. M. Padial, J. García-Martínez, N. Linares, D. Maspoch, J. A. Suárez Del Pino, P. Moghadam, R. Oktavian, R. E. Morris, P. S. Wheatley, J. Navarro, C. Petit, D. Danaci, M. J. Rosseinsky, A. P. Katsoulidis, M. Schröder, X. Han, S. Yang, C. Serre, G. Mouchaham, D. S. Sholl, R. Thyagarajan, D. Siderius, R. Q. Snurr, R. B. Goncalves, S. Telfer, S. J. Lee, V. P. Ting, J. L. Rowlandson, T. Uemura, T. Iiyuka, M. A. Van Der Veen, D. Rega, V. Van Speybroeck, S. M. J. Rogge, A. Lamaire, K. S. Walton, L. W. Bingel, S. Wuttke, J. Andreo, O. Yaghi, B. Zhang, C. T. Yavuz, T. S. Nguyen, F. Zamora, C. Montoro, H. Zhou, A. Kirchon and D. Fairen-Jimenez, *Adv. Mater.*, 2022, **34**, 2201502.

17 (*a*) M. Hmadeh, Z. Lu, Z. Liu, F. Gándara, H. Furukawa, S. Wan, V. Augustyn, R. Chang, L. Liao and F. Zhou, *Chem. Mater.*, 2012, **24**, 3511–3513; (*b*) A. Barthram, R. Cleary and M. Ward, *Chem. Commun.*, 1998, 2695–2696; (*c*) J. Y. Chan, E. O. Shehayeb, D. L. Pennington, C. H. Hendon and K. A. Mirica, *J. Am. Chem. Soc.*, 2025, **147**, 29003–29012; (*d*) H.-J. Noh, E. Cline, D. L. Pennington, H.-Y. G. Lin, C. H. Hendon and K. A. Mirica, *J. Am. Chem. Soc.*, 2025, **147**, 8240–8249; (*e*) H. J. Noh, D. L. Pennington, J. M. Seo, E. Cline, G. Benedetto, J. B. Baek, C. H. Hendon and K. A. Mirica, *Angew. Chem., Int. Ed.*, 2025, **64**, e202419869; (*f*) K. M. Snook, L. B. Zasada, D. Chehada and D. J. Xiao, *Chem. Sci.*, 2022, **13**, 10472–10478.